Countercurrent Gas–Solid Trickle Flow Reactor with Structured Packing: Hydrodynamics and CaO–CO_2 Reaction

Ana Obradović
Laboratory for Catalysis and Chemical Reaction Engineering, National Institute of Chemistry, Hajdrihova 19, 1000 Ljubljana, Slovenia

Janez Levec
Laboratory for Catalysis and Chemical Reaction Engineering, National Institute of Chemistry, Hajdrihova 19, 1000 Ljubljana, Slovenia

Faculty of Chemistry and Chemical Technology, University of Ljubljana, Aškerčeva cesta 5, 1000 Ljubljana, Slovenia

DOI 10.1002/aic.14731
Published online February 8, 2015 in Wiley Online Library (wileyonlinelibrary.com)

The sorption reaction CaO–CO_2 was examined in a countercurrent gas–solid trickle flow reactor with regularly stacked packing at T = 500–600°C, p_{CO2} = 40–50 kPa, solid-phase fluxes S = 0.3–0.5 kg m^{-2} s^{-1}, and CaO particles of 500–710 μm in size. Sorption kinetics was evaluated by thermogravimetric (TG) technique. The random pore model was used for the description of the carbonization reaction. Hydrodynamic characteristics of gas–solid trickle flow were estimated at room temperature and ambient pressure. Plug flow model of both gas and solid-phase, with the parameters obtained from TG and hydrodynamics experiments, satisfactorily described the sorption process in countercurrent gas–solid trickle flow reactor. © 2015 American Institute of Chemical Engineers *AIChE J*, 61: 1601–1612, 2015
Keywords: CaO–CO_2 reaction, hydrodynamics, countercurrent gas–solid trickle flow, structured packing, plug flow model

Introduction

In a gas–solid trickle flow system, solid-phase continuously flows downward through a packing, while the stream of gas is in most cases directed upwards. This type of flow can be successfully applied in adsorption and chemical reaction systems, because of the advantages it offers–low pressure drop, low level of axial mixing for both phases, and high rates of heat and mass transfer.[1,2] The packing in gas–solid trickle bed reactor may be in the form of Pall or Raschig rings, but Verver and van Swaaij[3] found that regularly stacked packing further minimized pressure drop and static solids hold-up, and provided rapid radial solid distribution throughout the column. Recently, Obradović et al.[4,5] introduced a novel structured plate-type catalyst in the form of a static mixer with corrugated plates, which is an excellent example of the regularly stacked type packing described above. Static mixers with corrugated plates (e.g., the SMV mixer) induce intense radial mixing for shortest space requirements.[6]

The need to reduce greenhouse gas emissions, including CO_2, represents a major driving force in improving the technologies being used for coal combustion and gasification processes. One of the most promising approaches involves the separation of CO_2 with a metal oxide, such as CaO.[7] Sorption-enhanced-steam methane reforming (SE–SMR) process is also an example where one can efficiently use the countercurrent flow of solid sorbent (e.g., CaO) and gaseous stream of CH_4 and H_2O in a reactor with a fixed bed of catalyst, which could be in a form of static mixers. The formed CO_2 in SMR simultaneously reacts with the sorbent and thus shifts the equilibrium limited reforming reactions to the product side, that is, toward hydrogen.[8]

In this work, the process of CO_2 sorption on CaO (as a part of the SE–SMR process) was studied in a countercurrent gas–solid trickle flow reactor, which was packed with inert structured packing elements. Prior to the sorption experiments, the hydrodynamics study in a cold plexiglas mockup as well as CaO–CO_2 reaction kinetic study were performed, so that the operation window could be determined for the sorption experiments. The sorption process conditions (temperature, CO_2 partial pressure, and flow rates of gas- and solid-phase) used in this work were the same as the ones usually encountered in SE–SMR.

Experimental

CaO–CO_2 reaction

Limestone (Table 1) for the reaction experiments was provided by a local quarry (Solkanska Industrija Apna, Nova Gorica, Slovenia). The limestone was crashed and a fraction 500–710 μm was sieved for the carbonation reaction study, which was performed in an atmospheric-pressure

Correspondence concerning this article should be addressed to: J. Levec at janez.levec@ki.si

Table 1. Chemical Composition of the Sorbent Used in the TGA Study

Constituent	wt.%
Ca	67 mg kg^{-1}
Constituent	mg kg^{-1}
Mg	3574
Si	413
Fe	133
S	243
Mn	12
Sr	311
Ba	3
Na	100
K	52
Al	220

thermogravimetric analyzer (TGA, Netzsch STA 449 F3 Jupiter, Germany). The mass of the sorbent was around 2 mg for each experimental run. Calcination of the sorbent sample in a flow of Ar ($Q = 50$ mL_{STP} min^{-1}, $h.r. = 20°C$ min^{-1}, $T = 840°C$, $t = 5$ min) was completed each time prior to the reaction experiments, which were performed in the following range: $T = 500–600°C$, $p_{CO2} = 4–12$ kPa, $Q_{total} = 250$ mL_{STP} min^{-1}, and $t = 15$ min. The experiments carried out beforehand assured that no external mass-transfer resistance was present at the total flow rate of 250 mL_{STP} min^{-1} and $p_{CO2} \leq 12$ kPa. The partial pressures of CO_2 were acquired by adjusting the mass flow controllers for Ar and CO_2 at the fixed total flow rate. The sample weight and temperature were continuously recorded, and the data were corrected by subtracting the results obtained from the preliminary blank tests. The calcined sorbent was characterized by a Hg Porosimeter (AutoPore IV 9500, Micromeritics) in the pressure range 1.6 kPa–414 MPa.

Hydrodynamic characteristics of solid-phase flow

The experimental setup for hydrodynamic measurements is the mockup version of the one depicted for reactive flow in Figure 1. It consisted of a plexi-glass tube packed with 10 structured elements (SMV static mixers, Sulzer Chemtech, Switzerland), 42 mm long and 43.1 mm in diameter. The hydraulic diameter and porosity of the element, as provided from the supplier, were 4.3 mm and 0.83, respectively. After every second element, a spacing (i.e., a ring with the fixed outer diameter of 43.1 mm and the inner diameter conically reduced from 43.1 to 32 mm in a distance of 10 mm) was inserted to redistribute the solids from the wall back to the column core. Above this tube, three SMV elements along with two spacings described above (after the first and the third SMV element, counting from the top) were used for establishing the initial solid flow distribution. The effect of the spacings for radial uniformity of the solid-phase within the column was confirmed by the experiments with a honeycomb element (50 mm in diameter and height, with 55 channels, 4 mm in diameter) with the closed bottom that was put for this purpose under the column part. The height of the channels filled with the solid material in the honeycomb element was measured in a certain period of time, and a picture of the radial distribution was in this way obtained at zero gas flow. Particular attention was given to the construction of the bin and the feeder for the solid-phase. Conical bin had a slope of 60°, whereas feeder was designed as a gear wheel of 70 mm in diameter and 20 mm in width. Twenty half-cylindrical grooves of radius 4 mm were equally spanned around the wheel circumference. The wheel was driven by an asynchronous motor (Siemens, Czech Republic), with the frequency 50 Hz/ 60 Hz. A magnetic coupling (Dexter

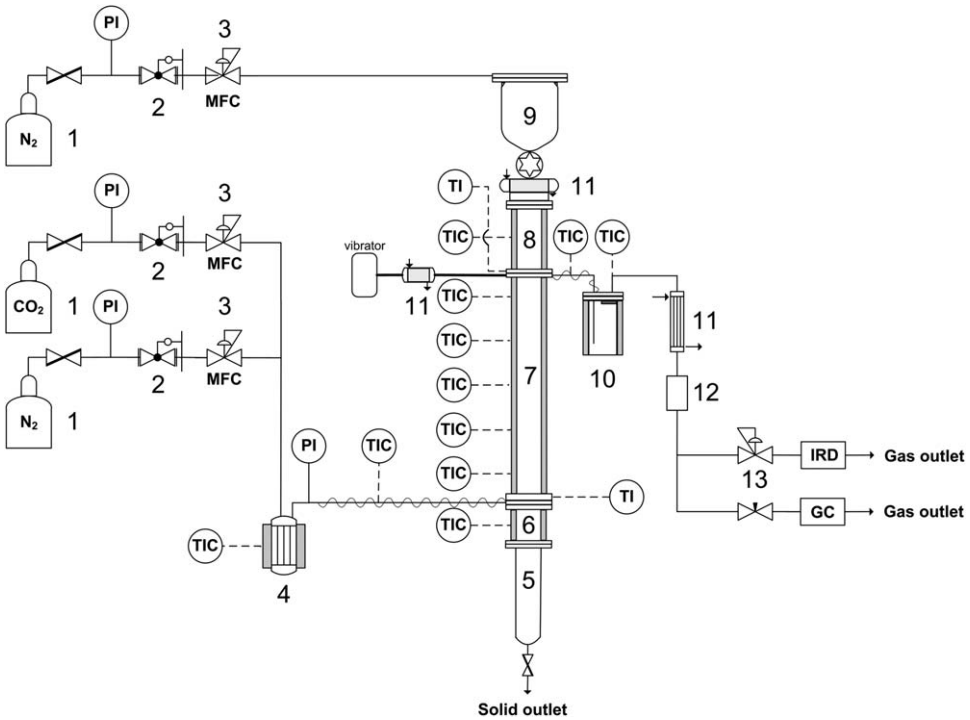

Figure 1. Schematics diagram of sorption experimental setup: (1) gas cylinders, (2) pressure reducers, (3) mass flow controllers, (4) gas preheating section, (5) vessel for collecting solids, (6) zone preventing gas-phase recirculation, (7) reaction zone with structured packing, (8) solid preheating and distribution zone, (9) bin, (10) filter, (11) coolers, (12) buffer, and (13) back pressure regulator.

Magnetic Technologies), with the torque 3 Nm, was interposed between the wheel and the motor. The motor speed was controlled by an inverter (FRENIC–Mini, Fuji Electric Corporation of America). At the column exit for the solid-phase, a special four-way valve was installed, which served as a flow diverter. The pressure drop was measured with the micro manometer (Wilh. LAMBRECHT GmbH, Germany).

The experiments were performed at the room temperature and pressure. Air and helium were used in the range 0–19 L_{STP} min^{-1} and the feed flow rate was controlled by mass flow controllers (MKS Instruments). To compare the solid-phase flowability through the SMV packing, two different solid materials, CaO and SiO_2, sieved in the fraction 500–710 μm, were used in the study. The wheel speed was in the range 0–50 rpm, which provided solid delivery rates up to 3.5 g s^{-1} for CaO, and 5.9 g s^{-1} for SiO_2. A micro vibrator (TIBA Elektromotorji, Slovenia), which was screwed tightly on the flange (Figure 1), provided appropriate working vibration with the frequency of 50 Hz, and a half-disc shaped 20 g eccentric weight attached on each end of a shaft for the experiments with SiO_2, and twice the weight for the experiments with CaO. The vibrations, with the centrifugal force of 1.36 and 2.72 N for the experiments with SiO_2 and CaO, respectively, enabled the operation of the gas–solid flow with minimized static solid holdup.

The experimental procedure was as follows: once a steady-state flow of both phases within the column was achieved, the pressure drop was written down. Then the gas and solid flow were simultaneously stopped and the four-way valve turned in the other direction, so that the solid-phase, which occupied the space between the solids feeder and the exit of the four-way valve, was collected in a sampling vessel. The reason why there was a four-way valve instead of a three-way one was to measure the amount of the solid-phase in the very valve, by turning the valve in the position that would have no connection with the column. The amount of the solid collected in the vessel minus the amount in the valve was considered the dynamic holdup of the solid-phase in the column for certain conditions. Before going to the higher values of the solid flow rates, the column was cleaned and the amount of the solid-phase collected, that is, the one that could not flow freely from the column once the solid- and gas-phase flows were stopped, but rested on the packing, was considered the static holdup.

Countercurrent sorption study

The experimental setup for the countercurrent sorption study is depicted in Figure 1. Namely, the reaction between trickling CaO particles and CO_2 took place in a 316Ti tube, packed with 10 SMV elements and spacings–redistributors, as described above. The tube was divided into five segments (for easier handling) and was heated by five heating elements with the total power of 3.8 kW. Thermocouples were installed in each of the five segments, and their tips were positioned only 1 mm from the reactor wall, in order not to disturb the solid-phase flow. The total packing length, which offered the contact between the gas-phase and the solid sorbent, was $L = 460$ mm (10×42 mm $+ 4 \times 10$ mm). Above the reaction zone, three SMV elements, along with two spacings, were used for preheating (1.2 kW) the falling solids and establishing the initial solid-phase distribution at the entrance of the reaction zone for the sorbent. Below the plane at which the gas-phase was introduced into the column, one additional SMV element was installed to prevent the recirculation of the gas-phase in this region. This part was also heated (1 kW). The whole column was isolated by an appropriate material. To minimize the heat flow from the hot apparatus to the surrounding frame, the joints were being cooled by a forced flow of cool water. On the column, a vibrator was mounted, with the same centrifugal force as described above for the cold flow experiments with CaO. Between the preheating zone for the sorbent, and the sorbent feeder, a cooler was inserted to prevent heat conduction to the feeder. A very important feature of the apparatus was feeding N_2 by a mass flow controller (Brooks 5850TR) to the top of the bin in the amount of 10 vol % of the total volume flow in the reaction zone, to minimize the diffusion of the gases from the reaction zone to the preheating zone and bin. Also, in that way, the feeding of the sorbent proceeded with no obstacles regarding the pressure. The sorbent used in the sorption study was two times calcined CaO of the fraction 500–710 μm, from different batch than the one used in the TGA reaction study. The calcinations of the sorbent were performed in the circulating atmosphere of N_2 in the Nabertherm furnace (Germany) for 10 min at the temperature of 840°C (h.r. 10°C min^{-1}). The mixture of CO_2 and N_2 that were controllably fed (Brooks 5850TR) was preheated to the reaction temperature before entering the column at the bottom of the reaction zone. The total pressure was in the range 150–180 kPa, whereas the partial pressure of CO_2 at the gas-phase entrance was 40 and 50 kPa. The experiments were performed at the reaction temperature of 500 and 600°C, total flow rate range 2–5 L_{STP} min^{-1}, and CaO flux of 0.3 and 0.5 kg m^{-2} s^{-1}. Concentration of CO_2 in the outlet gas stream was monitored continuously by an infrared (IR) analyzer (Binos 1001, Rosemount, MN). Part of the outlet gas stream was also analyzed by a gas chromatograph (Agilent 7890A GC System, USA) for CO_2 and N_2.

The experimental procedure was the following one: after a steady state was achieved with the gas-phase mixture of CO_2 and N_2, the sorbent feeding was started. Once the steady state was achieved in the reactor zone (no more decline in the concentration of CO_2 in the outlet stream detected by the IR analyzer), the sample for GC was taken. After that, the solid sorbent flow was stopped, and the preparation of the gas mixture for a new experiment was begun.

Results and Discussion

CaO–CO_2 reaction parameter estimation

The carbonization reaction process proceeds in two stages: chemically controlled initial reaction stage, followed by an abrupt slower reaction stage controlled by the diffusion in the product ($CaCO_3$) layer. Semiempirical (apparent) models,[9] shrinking core model,[10] random pore model (RPM),[11,12] and grain model[13] are some of the ways for modelling the carbonization process. However, RPM has the advantage of incorporating textural properties of fresh (1× calcined) CaO that can be calculated through readily measurable pore-size distribution of the sorbent by mercury porosimetry technique.[11] The carbonation conversion of CaO can be calculated from the TGA data as follows

$$X = \frac{(m_t - m_0)}{m_0 \times w} \frac{M_{CaO}}{M_{CO_2}} \tag{1}$$

where m_0 is the mass of the calcined sample in the TGA basket, m_t is the mass of the sample at time t, w is the

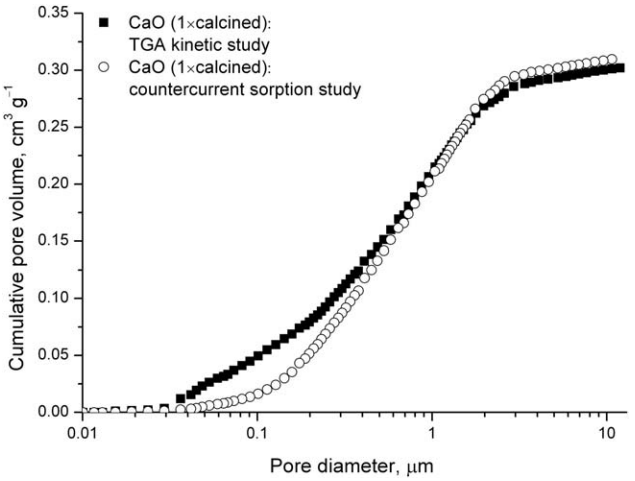

Figure 2. Cumulative pore volume curves for the sorbents used.

weight fraction of CaO in the calcined sorbent ($w = 0.937$ in this study), and M_{CaO} and M_{CO2} are the molar weights of CaO and CO_2, respectively. The cumulative pore volume curves obtained by mercury porosimetry for fresh (1× calcined) sorbents used in the TGA and in the gas–solid countercurrent sorption study are depicted in Figure 2. Different batches resulted in slightly different curves.

According to the RPM proposed by Bhatia and Perlmutter,[11] general expression for the sorbent conversion rate can be written as

$$\frac{dX}{dt} = \frac{k_s S_0 C(1-X)\sqrt{1-\psi\ln(1-X)}}{(1-\varepsilon_0)\left[1+\frac{\beta Z}{\psi}\left(\sqrt{1-\psi\ln(1-X)}-1\right)\right]} \tag{2}$$

where ψ is a structural parameter defined by

$$\psi = \frac{4\pi L_0(1-\varepsilon_0)}{S_0^2} \tag{3}$$

with L_0 and S_0 being the initial total length and surface area per unit volume, respectively, ε_0 the initial porosity of the fresh (1× calcined) sorbent, and C the local concentration of CO_2. These parameters can be calculated from the mercury porosimetry data as

$$L_0 = \int_0^\infty \frac{v_0(r)}{\pi r^2} dr \tag{4}$$

$$S_0 = 2\int_0^\infty \frac{v_0(r)}{r} dr \tag{5}$$

$$\varepsilon_0 = \int_0^\infty v_0(r) dr \tag{6}$$

where $v_0(r)$ is the pore radii distribution of the fresh sorbent.

The modified Biot modulus, β, in Eq. 2 is defined as

$$\beta = \frac{2k_s\rho(1-\varepsilon_0)}{M_{CaO} D S_0} \tag{7}$$

where ρ is the mass of CaO per unit volume of solid-phase, k_s is rate constant for the surface reaction, and D is the effective product layer diffusivity. The molar volume ratio of the carbonation product to that of the reactant, Z, in Eq. 2 can be written as

$$Z = \frac{\frac{M_{CaCO_3}}{\rho_{CaCO_3}} + \frac{M_{CaO}(1-w)}{w\rho_{sorbent}}}{\frac{M_{CaO}}{\rho_{CaO}} + \frac{M_{CaO}(1-w)}{w\rho_{sorbent}}} \tag{8}$$

with $\rho_{sorbent}$ being the solid sorbent density. The structural parameters of the sorbents used are listed in Table 2.

Previous studies have shown that the carbonation reaction is first order with respect to the CO_2 concentrations.[14–19] In the fast stage of chemical reaction control for the reversible first-order system with no external transport resistance, the general expression Eq. 2 can be simplified, since $D >> k_s$, that is, $\beta \to 0$

$$\frac{dX}{dt} = \frac{k_s S_0 (C_b - C_{eq})(1-X)\sqrt{1-\psi\ln(1-X)}}{(1-\varepsilon_0)} \tag{9}$$

where C_b and C_{eq} are the concentration in the bulk fluid and equilibrium one of CO_2, respectively. In the reaction stage with the product layer diffusion control, $k_s >> D$, that is, $\beta \to +\infty$, and the simplification leads to

$$\frac{dX}{dt} = \frac{M_{CaO} D C_b S_0^2 \psi (1-X)\sqrt{1-\psi\ln(1-X)}}{2\rho Z(1-\varepsilon_0)^2\left(\sqrt{1-\psi\ln(1-X)}-1\right)} \tag{10}$$

It should be observed that both Eqs. 9 and 10 have just one parameter unknown, that is, k_s and D, respectively, with other parameters calculated from the mercury porosimetry data, as presented in Table 2. Equations 9 and 10 describe the process if no diffusional resistance within the particle is encountered. However, as the particles used in this study were from the sieve fraction 500–710 μm, it was necessary to compare the results for k_s and D obtained when no diffusional resistance was assumed within the particle, and those with supposing the diffusional resistance within the particle existed. For the case when diffusional resistance within the particle is accounted for, Eqs. 9 and 10 (with C_b now replaced by C that is dependent on the position within the particle) should be simultaneously solved with the equation representing diffusion in a spherical particle[12]

$$\frac{1}{R^2}\frac{\partial}{\partial R}\left(D_e R^2 \frac{\partial C}{\partial R}\right) = \frac{\rho(1-\varepsilon_0)}{M_{CaO}}\frac{dX}{dt} \tag{11}$$

with R and D_e being the radial position within the particle, and effective diffusivity, respectively. The boundary conditions for Eq. 11, if no external mass-transfer resistance is present, are

$$\frac{\partial C}{\partial R} = 0 \text{ at } R = 0 \tag{12}$$

$$C = C_b \text{ at } R = R_0 \tag{13}$$

According to the model of Wakao and Smith,[20] the effective diffusivity varies with the structural parameters of the solid in the form

$$D_e = \bar{D}\varepsilon^2 \tag{14}$$

where the equivalent diffusion coefficient is typically described using Bosanquet equation

$$\bar{D} = \left(\frac{1}{D_m} + \frac{1}{D_k}\right)^{-1} \tag{15}$$

with D_m and D_k being molecular and Knudsen components of the diffusivity, the latter calculated for the average pore

Table 2. Structural Characteristics of the Fresh (1× Calcined) Sorbents Used in the Study

	S_0 ($m^2\ m^{-3}$)	L_0 ($m\ m^{-3}$)	ε_0	ψ	Z	$\rho_{sorbent}$ ($g\ cm^{-3}$)	d_{pore} (nm)
TGA study	10.6×10^6	6.60×10^{13}	0.4685	3.93	2.12	2.88	412.6
Countercurrent study	6.3×10^6	2.29×10^{13}	0.4847	3.75	2.12	3.02	759.0

diameter provided in Table 2 (TGA study). In the binary gas mixtures, D_m can be predicted by the Chapman Enskog theory.[21] The porosity in Eq. 14 changes with conversion as

$$\varepsilon=\varepsilon_0-(Z-1)(1-\varepsilon_0)X \tag{16}$$

If no diffusional resistance within the particle was assumed, k_s and D in Eqs. 9 and 10 were estimated from the experimental values using the Levenberg–Marquardt optimization procedure, coupled with the Runge–Kutta method for the integration of the differential equations (Eqs. 9 and 10). All the calculations in this study were performed by means of Matlab R2011a software (Mathworks, Natick, MA).

Supposing the diffusional resistance within the particle existed, the Eqs. 9 and 11–16 or 10 and 11–16, had to be solved simultaneously, to optimize the parameters (k_s and D) by comparing experimental and calculated conversions. It was assumed that the sorbent particle was of a spherical shape with the average particle diameter of 605 μm, and that there was no heat-transfer resistance within the particle. The equations, presented in the dimensionless form in Table 3, were solved numerically by orthogonal collocation technique based on the Legendre polynomials,[22,23] using 8 or less collocation points. In that way the partial differential equation was transformed into a system of linear algebraic equations and simultaneously solved with the rate equation, which was integrated using the Runge–Kutta method. Again, the optimization was done using the Levenberg–Marquardt optimization procedure. The overall conversion in the particle was calculated from the equation

$$X_{overall}=3\int_0^1 X\eta^2 d\eta \tag{17}$$

with η being the dimensionless radius defined in Table 3.

The rate constant, k_s, can be expressed by the Arrhenius equation

$$k_s=k_{s0}\ \exp(-E_a/(RT)) \tag{18}$$

As shown in Figure 3, the diffusion resistance within the particle does not affect much the overall reaction rate, since there is just a slight difference between ln k_s values (y axis) obtained with or without assumed particle diffusion in the model. However, the higher values for k_s were taken for intrinsic, with the parameter values, k_{s0} and E_a, given in Table 4 with 95% confidence intervals.

Some of the experimental values of the overall CaO conversion (Eq. 1) along with the simulated curves are shown in Figure 4. The values for k_s and E_a agree well with those observed in the earlier studies.[14,18,19] However, it should be noted that the activation energy is very low (Table 4 and Figure 4b), which may explain the fact why Bhatia and Perlmutter[14] considered it to be zero activation energy in their study. The intrinsic values for the product layer diffusivity, D, are shown in Table 4. Similarly, very small difference in values, with or without diffusion assumed in the particle, was observed. Comparison was made between the experimental and calculated values of conversion in Figure 5.

Contrary to some earlier studies,[18,19] D could not be expressed by the Arrhenius equation in this study. Bhatia and Perlmutter[14] observed change in the activation energy for the diffusion in the product layer at 788 K. They explained the phenomenon by change in the mechanism near the Tammann temperature. Namely, at lower temperatures, CO_3^{-2} was accepted to be the mobile species in ionic conduction through $CaCO_3$, with the countercurrent motion of O^{-2}, whereas at the temperatures above 788 K, it was presumed that the higher rates of CO_2 diffusion through $CaCO_3$ layer were due to CO_3^{-2} ion decomposition

Table 3. Set of Equations Describing Conversion Process with Diffusional Resistance Within the Particle

Chemically controlled reaction stage	Product layer diffusion controlled reaction stage
$\frac{1}{\eta^2}\frac{\partial}{\partial\eta}\left(D_e^*\eta^2\frac{\partial C^*}{\partial\eta}\right)=\phi^2\frac{dX}{d\tau}$	$\frac{1}{\eta^2}\frac{\partial}{\partial\eta}\left(D_e^*\eta^2\frac{\partial C^*}{\partial\eta}\right)=\phi^2\frac{dX}{d\tau}$
$\frac{dX}{d\tau}=(C^*-C_e^*)(1-X)\sqrt{1-\psi\ln(1-X)}$	$\frac{dX}{d\tau}=\frac{C^*\psi(1-X)\sqrt{1-\psi\ln(1-X)}}{2Z\left(\sqrt{1-\psi\ln(1-X)}-1\right)}$
Boundary conditions	Boundary conditions
$\frac{\partial C^*}{\partial\eta}=0$ at $\eta=0$	$\frac{\partial C^*}{\partial\eta}=0$ at $\eta=0$
$C^*=1$ at $\eta=1$	$C^*=1$ at $\eta=1$
Initial condition	Initial condition[a]
$X=0$ at $\tau=0$, for $0\le\eta\le1$	$X(p,t)=X(p,t_1)$ at $t=t_1$, for $p=1,...,N+1$
	$N-$ no. of collocation points
$\phi=R_0\sqrt{\frac{k_s\rho S_0}{M_{CaO}D_{e0}}}$ $\quad\tau=\frac{k_sC_bS_0t}{(1-\varepsilon_0)}$	$\phi=R_0S_0\sqrt{\frac{D}{D_{e0}(1-\varepsilon_0)}}$ $\quad\tau=\frac{M_{CaO}DC_bS_0^2t}{\rho(1-\varepsilon_0)^2}$
$C_{(e)}^*=\frac{C_{(e)}}{C_b}$ $\quad\eta=\frac{R}{R_0}$ $\quad D_e^*=(\varepsilon^*)^2$ $\quad\varepsilon^*=1-\frac{(Z-1)(1-\varepsilon_0)X}{\varepsilon_0}$ $\quad D_e^*=\frac{D_e}{D_{e0}}$ $\quad\varepsilon^*=\frac{\varepsilon}{\varepsilon_0}$	

[a]$X(p,t_1)$ obtained from the chemically controlled reaction stage at experimental time, t_1, assuming that sharp transition between the two reaction stages occurs.

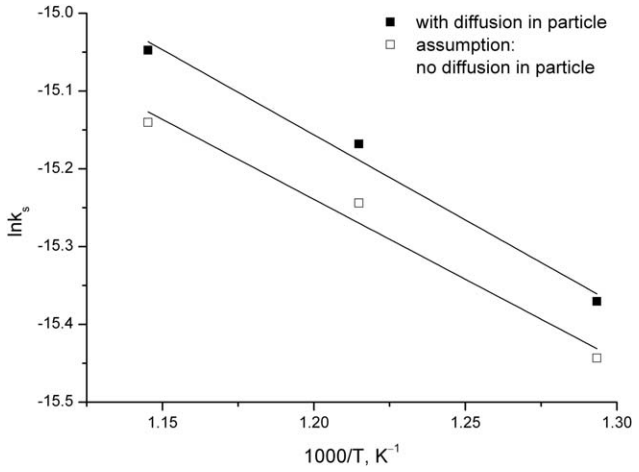

Figure 3. Effect of temperature and diffusion on sorption kinetic rate constant.

to carbon dioxide and an oxygen ion. It was speculated that this CO_2 molecule further moved to a neighboring similarly vacated site, while another CO_2 so produced elsewhere moved to take its place and reform the CO_3^{-2} ion.[14]

It should be noted here that the main purpose of this CaO–CO_2 reaction study was to describe the sorption process taking place in the kinetically controlled regime, since the particles falling down in the countercurrent sorption experiments were in this regime.

Hydrodynamic characteristics of solid-phase flow

Before the hydrodynamic study was performed, it was checked whether the radial uniformity of the solid-phase could be established within the column. Namely, it was observed that with the spacings–redistributors (described in the Experimental Section) added, the radial profile uniformity was improved, as shown in Figure 6. Therefore, all the following experiments were done with the spacings in the column.

In the gas–solid trickle bed columns, three possible operating zones were reported in the literature, called "preloading region," "loading zone," and "flooding point." In the preloading region, the amount of solid-phase per unit of the cross-sectional area of the column has been observed to be independent of the gas and the solids flow rates.[24] For the experimental conditions in this study, the hydrodynamic experiments with both CaO and SiO_2 showed that the preloading regime was established within the column. The mean particle velocity for the preloading zone can be calculated as[25]

$$u_p^o = \frac{S}{\rho_p \beta_{dyn}} \tag{19}$$

where S is the solid-phase flow rate per unit of cross-sectional area of the empty column, ρ_p is the particle density (Table 5), and β_{dyn} is the dynamic holdup, defined as the volume occupied by the solids flowing in the column per unit volume of the empty column. The results with the dynamic holdup for CaO and SiO_2 are presented in Figure 7, from which the mean particle velocity (Eq. 19) was obtained.

The values of the mean particle velocities for CaO and SiO_2 are presented in Table 5. For the Reynolds numbers between 2 and 500 (transition regime), the terminal particle velocity, that is, the maximum velocity of the falling particle, can be calculated from[26]

$$u_t = \left[\frac{(d_p)^{8/5}(\rho_p - \rho_g)g}{13.875(\rho_g)^{2/5}(\mu_g)^{3/5}}\right]^{5/7} \tag{20}$$

The values of the terminal velocities (in air at room temperature) for the two different solids, that is, CaO and SiO_2, are also presented in Table 5. It is interesting to observe that although the terminal velocity of the particles of CaO and SiO_2 is different because of the different particle density, the mean particle velocity is the same for the two solids. This suggests that the solid particle interaction with the SMV packing in the column, that is, the geometry of the packing, is crucial for the duration of the solid travelling through the column.

The experimental results for the static holdup, β_{st}, are shown in Figure 8, with and without the vibrations applied. Static holdup is defined per unit volume of the empty column as the volume of the column occupied by the solids that rest on the packing and do not flow out of the column once the flow of the solids is stopped. It can be observed that there is just a slight difference in the value of β_{st} for CaO with and without vibrations applied, whereas for SiO_2 a bigger difference is observed. It can be also noticed that with increasing S, β_{st} for SiO_2 would have finally reached a plateau, whereas with CaO, β_{st} and S were linearly dependent. This indicates a more "sticky" nature of CaO material compared to that of SiO_2.

The pressure drop without trickle experiments, that is, the pressure drop on packing, can be predicted using the Ergun equation formulation

$$\frac{\Delta P}{L} = C_1 \frac{u_g \mu_g (1-\varepsilon_{pack})^2}{d_{pack}^2 \varepsilon_{pack}^3} + C_2 \frac{\rho_g u_g^2}{d_{pack}} \frac{1-\varepsilon_{pack}}{\varepsilon_{pack}^3} \tag{21}$$

with $C_1 = 150$ and $C_2 = 1.75$ in the original form, u_g being the superficial gas velocity, μ_g the dynamic viscosity of the gas-phase, d_{pack} the diameter of a packing particle, and ε_{pack} the void fraction of packing. In case of structured packing, nominal diameter of the packing should be used for d_{pack}, which can be expressed through the hydraulic diameter, d_H, defined as

$$d_H = \frac{4\times \text{ void volume of medium}}{\text{surface area of channels in medium}} \tag{22}$$

From Eq. 22, d_{pack} can be calculated as

$$d_{pack} = \frac{3}{2}\frac{(1-\varepsilon_{pack})}{\varepsilon_{pack}} d_H \tag{23}$$

According to Eq. 21, the pressure gradient on the packing can be written using d_H as

Table 4. Kinetic and Product Layer Diffusion Parameters for RPM

k_{s0} (m^4 $kmol^{-1}$ s^{-1})	E_a (kJ mol^{-1})	D (500°C) (m^2 s^{-1})	D (550°C) (m^2 s^{-1})	D (600°C) (m^2 s^{-1})
$(3.6 \mp 0.9) \times 10^{-6}$	18 ± 2	$(6.77 \pm 0.04) \times 10^{-16}$	$(9.26 \pm 0.03) \times 10^{-16}$	$(5.003 \pm 0.002) \times 10^{-15}$

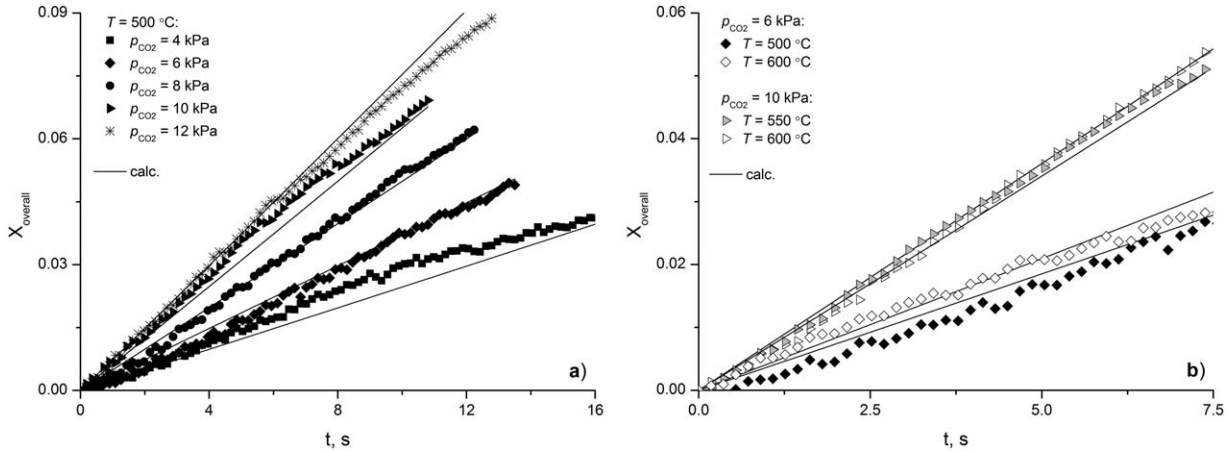

Figure 4. Comparison of experimental and calculated values of overall CaO conversion using RPM with intraparticle diffusion resistance.

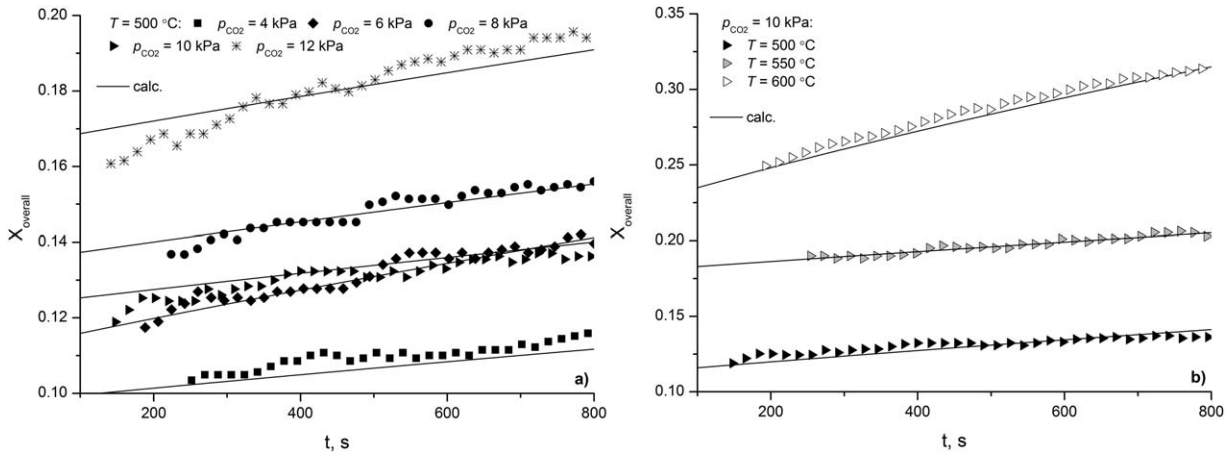

Figure 5. Comparison of experimental and calculated values of overall CaO conversion in the stage of reaction controlled by diffusion in product layer using RPM with intraparticle diffusion resistance.

$$\frac{\Delta P}{L}=\frac{4}{9}C_1\mathrm{Re}_{\mathrm{pack}}\frac{\mu_g^2}{\rho_g d_H^3}+\frac{2}{3}C_2\mathrm{Re}_{\mathrm{pack}}^2\frac{\mu_g^2}{\rho_g d_H^3} \tag{24}$$

with Reynolds number in the packing defined as

$$\mathrm{Re}_{\mathrm{pack}}=\frac{\rho_g u_g d_H}{\varepsilon_{\mathrm{pack}}\mu_g} \tag{25}$$

The coefficients C_1 and C_2 for the SMV packing in this study were found by fitting the curve to the experimental data ($S=0$), as shown in Figure 9. The values obtained (with 95% confidence intervals provided) were $C_1=68\pm14$ and $C_2=2.0\pm0.1$. These results are lower than those proposed by Ergun (150 and 1.75, respectively); however, they

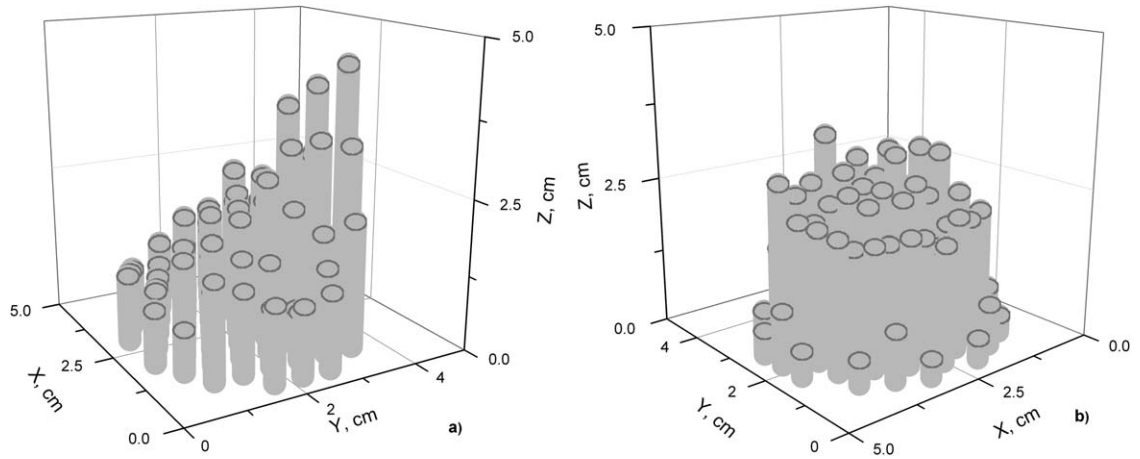

Figure 6. Typical graph of radial solids profile within column (a) without spacings, (b) with spacings.

Table 5. Terminal and Mean Particle Velocities of Falling Particles of CaO and SiO_2 for $d_p = 605$ μm

Solid	ρ_p (kg m^{-3})	u_t (m s^{-1})	u_p^o (m s^{-1})
CaO	1555	3.2	0.0905 ± 0.0008
SiO_2	2648	4.6	0.090 ± 0.001

are in agreement with the results obtained by Westerterp and Kuczynski[24] on the Kerapak packing, which is characterized by a regular geometry with no vertical channels. Although the experimental points with the trickle flow show somewhat higher pressure gradients (shown for SiO_2 only in Figure 9), the highest value for the same (at the highest S, u_g, and μ_g), was 56 Pa m^{-1}, which is still negligible, and can be, therefore, neglected in this study.

Countercurrent sorption study

In the countercurrent sorption study, 2× calcined sorbent was used. Since the average time needed for the particle to travel the distance of the reaction zone of $L = 0.46$ m was approximately 5 s, all the experiments were performed in the kinetically controlled regime.

Some earlier studies[16,18] have shown that the RPM can be successfully applied to a multicycle carbonation process, as well, without the need for mercury porosimetry measurements (after every calcination done) for the estimation of the structural parameters needed for the model. In fact, by knowing the structural parameters of the fresh calcine, structural parameters for multicycled calcines can be calculated using the following relations (for the first few cycles)[16]

$$S_N = S_0 X_N \tag{26}$$

$$L_N = L_0 X_N \tag{27}$$

where S_N and L_N denote reaction surface and pore length for cycle N, respectively, and X_N presents the sorbent carrying capacity with the number of cycles N, which is for a large number of limestones and conditions defined as[27]

$$X_N = \frac{1}{\frac{1}{(1-0.075)} + 0.52N} + 0.075 \tag{28}$$

So, with the value for S_0 and L_0 (Table 2, countercurrent study) for the fresh sorbent, S_1 and L_1 ($N = 1$) can be calculated from Eqs. 26 and 27, and then from Eq. 3, supposing that the overall porosity did not change, ψ_1 can be estimated. The kinetic rate constant, k_s, for the sorbent used in the countercurrent sorption study was taken the same as the one obtained in the CaO–CO_2 reaction study.

A typical response of the exit gas-phase composition after introducing CaO is shown in Figure 10. It should be noted that this gas-phase response to the step input of the solid-phase represents a composed function obtained as a result of the gas-phase passing through four vessels in row (Figure 1). Therefore, it could not be used for evaluating the reactor dynamics, but served only to determine the time period after which the steady-state operation was positively reached in the reactor. To describe the countercurrent sorption process in the steady-state operation, the following assumptions were made:

1. No diffusion resistance within the sorbent particle. From Table 2 it can be seen that the average pore diameter of the 1× calcined sorbent used was bigger than the one of the sorbent used in the CaO–CO_2 reaction study. For 2× calcined sorbent, the average pore diameter is even higher,[28]
2. The sorbent particles were spherical and uniform in size, with the diameter of 605 μm,
3. k_s (Table 4) was taken to be the same as the one obtained in the CaO–CO_2 reaction study. Equations 26–28 were used for predicting the structured parameters for the 2× calcined sorbent,
4. Solid particles flew downward in plug flow. This assumption can be justified since the spacings–redistributors were inserted (Figure 5), and also particles used in the study were coarse and the solids flow rates low, which had for the consequence negligible axial dispersion of the solid-phase,[29]
5. Gas-phase flew upwards in plug flow. This assumption is reasonable since the static mixers are known for inducing plug flow even for low Reynolds numbers,[6]
6. The reaction zone was considered as continuity with respect to the packing and spacings ($L = 0.46$ m),
7. The process was isothermal, which was also confirmed experimentally.

With the axial coordinate z taken as positive in the upward direction, the steady-state mass balances for both phases can be written as:

-for the reactant (CO_2) in the gas-phase

$$-\frac{d(C_g u_g)}{dz} - k_g a(C_g - C_{g,i}) = 0 \tag{29}$$

with the boundary condition

$$z = 0 \quad C_g = C_{g0} \tag{30}$$

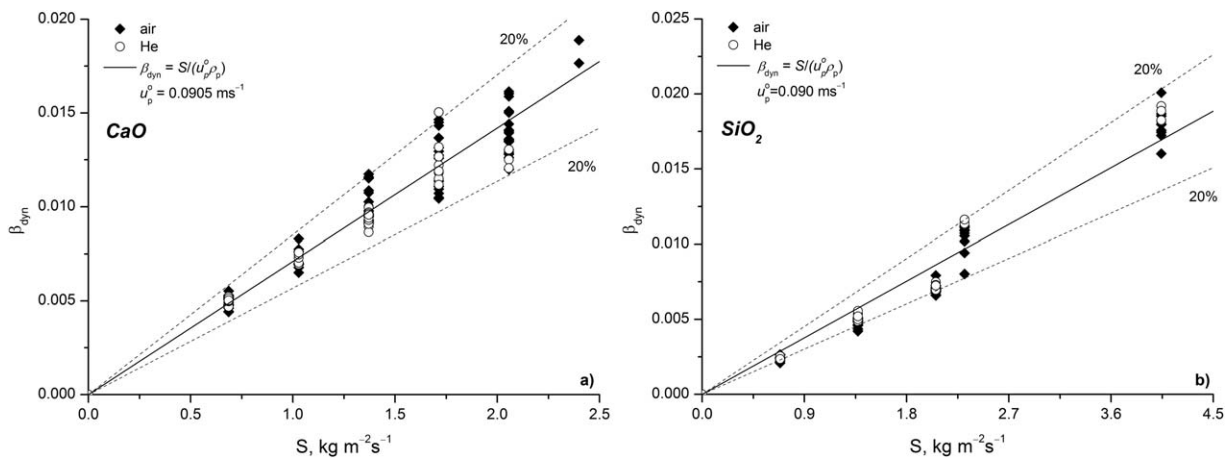

Figure 7. Dynamic holdup of solids as a function of solid-phase mass flux: (a) CaO, (b) SiO_2 particles.

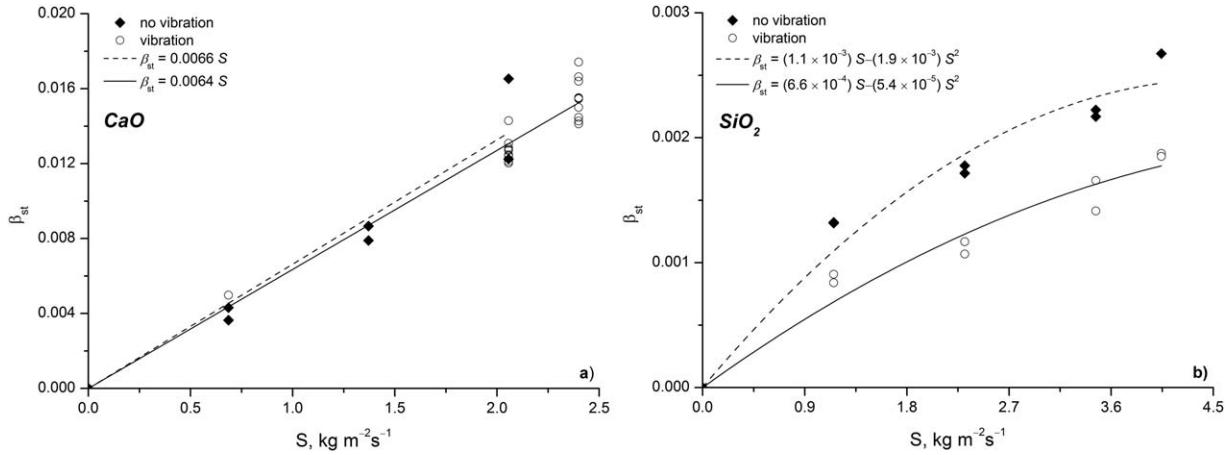

Figure 8. Static holdup of solids as a function of solid-phase mass flux: (a) CaO, (b) SiO_2 particles.

where C_g and $C_{g,i}$ are the concentration of CO_2 in the gas-phase and interface, u_g is the superficial velocity of the gas-phase, and k_g and a are the gas–solid mass-transfer coefficient and the specific interfacial area, respectively,

-for the solid reactant (CaO)

$$\frac{S}{\rho_p}\frac{dC_s}{dz} - \nu k_g a\left(C_g - C_{g,i}\right) = 0 \tag{31}$$

with the boundary condition

$$z = L \quad C_s = C_{s0} \tag{32}$$

where ν is the stoichiometric coefficient for CaO in the carbonization reaction ($\nu = 1$), ρ_p is the particle density, taken from Table 5 for CaO, and C_s is the concentration of the solid reactant.

To eliminate the unknown interface concentrations from Eqs. 29 and 31, the mass balance for CO_2 over the porous sorbent is introduced with RPM used

$$k_g a\left(C_g - C_{g,i}\right) = \beta_{dyn}\left(C_{g,i} - C_{g,eq}\right)\frac{k_s S_1 C_s\sqrt{1-\psi_1 \ln\left(\frac{C_s}{C_{s0}}\right)}}{1-\varepsilon_0} \tag{33}$$

Mass-transfer coefficient was estimated from the Ranz–Marshall correlation for a single particle in an undisturbed gas flow[30]

$$\mathrm{Sh} = \frac{k_g d_p}{D_m} = 2.0 + 0.6\mathrm{Re}_p^{1/2}\mathrm{Sc}^{1/3} \tag{34}$$

where Reynolds number was defined with the average local solids and gas velocities, as proposed by Kiel et al.[31]

$$\mathrm{Re}_p = \frac{\rho_g d_p \left| u_p^o - \frac{u_g}{\varepsilon_{pack}} \right|}{\mu_g} \tag{35}$$

The molecular diffusion coefficient, D_m, was predicted by the Chapman Enskog theory,[21] whereas gas viscosity by Chung et al. estimation method.[21] The superficial gas velocity was determined as

$$u_g = \frac{Q_{N_2}}{\left(D_{reactor}^2\pi/4\right)\left(1 - C_g RT/P\right)} \tag{36}$$

where Q_{N2} was the volumetric flow rate of N_2 in the reactor zone. The specific interfacial area was estimated as

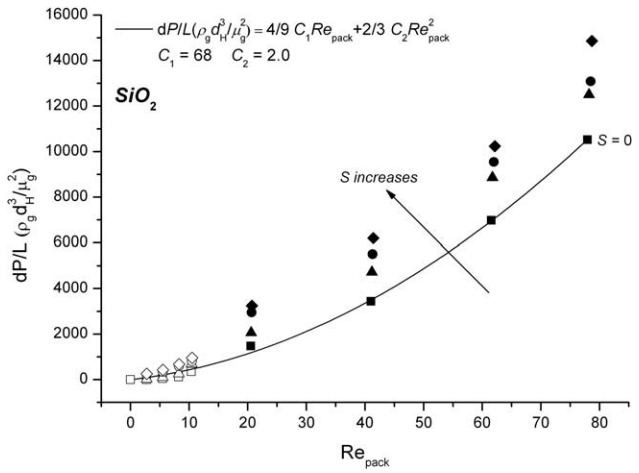

Figure 9. Pressure gradient in gas−solid trickle flow experiments with SiO_2.

Open and closed symbols denote experiments done with He and air, respectively.

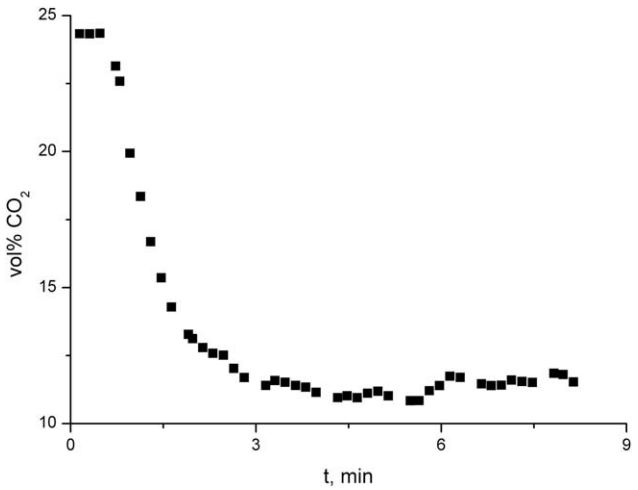

Figure 10. Typical sample response of the exit gas-phase composition after introducing CaO: approach to the steady state.

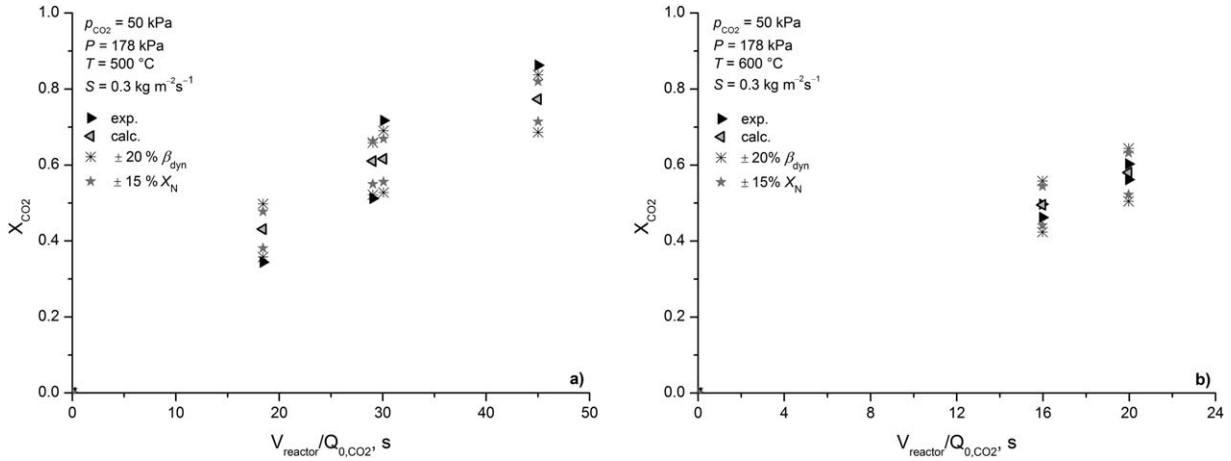

Figure 11. Conversion of CO_2 as a function of $V_{reactor}/Q_{CO2,0}$ at two different temperatures at lower solids flux.

$$a = \frac{6\beta_{dyn}}{d_p} \tag{37}$$

One should note that the gas viscosity, molecular diffusion, and gas velocity changed with z, as CO_2 was removed from the gas-phase.

Equations 29–37 were solved by forward-difference approximation in 10,000 points along the length of reaction zone. Initial guesses were made for C_g at $z = L$, until C_g calculated at the inlet was not equal to C_{g0}. The conversion of CO_2 was calculated then as

$$X_{CO_2,calc.} = \frac{(C_g u_g)|_{z=0} - (C_g u_g)|_{z=L}}{(C_g u_g)|_{z=0}} \tag{38}$$

and this value was compared to the experimentally obtained conversion of CO_2

$$X_{CO_2,exp.} = \frac{Q_{CO_2,0} - \frac{Q_{N_2,reactor}}{(1-y_{CO_2}|_{z=L})}(y_{CO_2}|_{z=L})}{Q_{CO_2,0}} \tag{39}$$

where $y_{CO2}|_{z=L}$ is the volume fraction of CO_2 at the outlet of the reactor, calculated from the CO_2 volume fraction measured at GC/IR, $y_{CO2}|_{GC/IR}$, as

$$y_{CO_2}|_{z=L} = \frac{Q_{N_2,reactor} + Q_{N_2,bin}}{\frac{Q_{N_2,reactor}}{y_{CO_2}|_{GC/IR}} + Q_{N_2,bin}} \tag{40}$$

where $Q_{N2,bin}$ is the volume flow rate of nitrogen through the bin. The above described conversions of CO_2 vs. the ratio of the reactor volume and CO_2 volumetric flow rates at the inlet are depicted in Figures 11 and 12. In Figure 11, all the experimental points were obtained at the same total pressure, whereas in Figure 12 the experiments were performed at different total pressures.

As one can observe, the model proposed (Eqs. 26–37) involves four parameters—the kinetic constant (k_s), dynamic solids holdup (β_{dyn}), maximum sorbent CO_2 capture capacity with the number of calcination/carbonation cycles (X_N), and mass transport coefficient (k_g). The first two were obtained from the separate experimental study, described previously. The sorbent carrying capacity with the number of cycles, X_N, was approximated from the relation proposed by Grasa and Abanades[27] (Eq. 28). Although the error introduced with the proposed correlation was not studied in the original work,[27] it could be estimated as ±15% for the first few carbonation/calcination cycles. Since the sorbent particle dimensions were relatively large and solid-phase fluxes low, high relative velocities were achieved in the system with a negligible influence of the particle shielding phenomena on mass transfer,[31] and the Ranz–Marshall correlation (Eq. 34) for the gas–solids mass-transfer coefficient could be therefore used as a good approximation for k_g. So, in this stage (countercurrent sorption) no parameter fitting was performed. The parameter sensitivity analysis showed that the error of

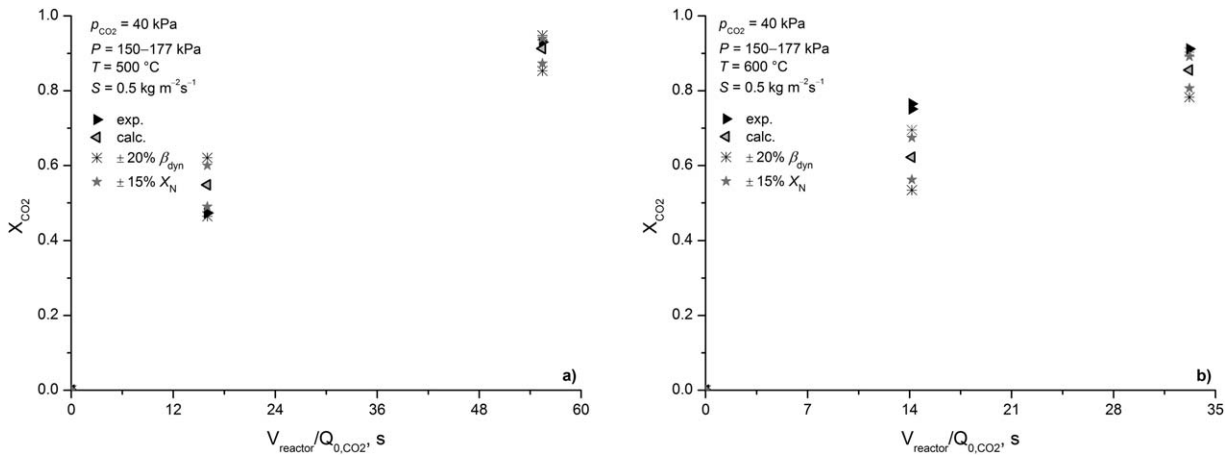

Figure 12. Conversion of CO_2 as a function of $V_{reactor}/Q_{CO2,0}$ at two different temperatures at higher solids flux.

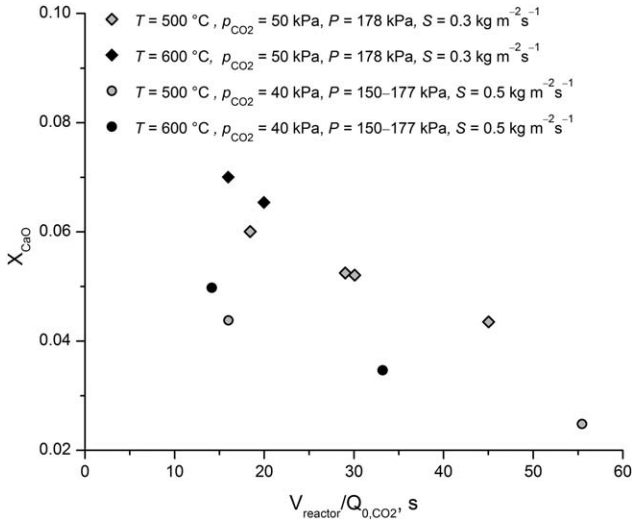

Figure 13. Calculated solid sorbent conversion at the reaction zone exit.

$\pm 20\%$ of β_{dyn} observed during the cold flow experiments (Figure 7) influenced most the experimental results for the countercurrent sorption (Figures 11 and 12). It should be noted that the sorption experiments were performed at a very low solid-phase flow rate, where the error for β_{dyn} might be even higher. Also, the possible propagation of error of the calculated data due to using the relation proposed for X_N (Eq. 28) was accounted for and shown in Figures 11 and 12. Particle conversion calculated at the reaction zone exit is depicted in Figure 13, where the effect of different gas-phase residence time (expressed through $V_{reactor}/Q_{CO2,0}$) is shown. Namely, a slight decrease in particle conversion (for constant partial pressure of CO_2 at the inlet of the reaction zone, total pressure, and temperature) can be ascribed to a combined influence of mass transfer and different CO_2 concentration in gas-phase along the reactor axis.

Conclusions

It was experimentally demonstrated in this study that the countercurrent reactive flow of CO_2/N_2 and CaO particles in a trickle flow reactor with structured packing can be successfully carried out. To understand and describe the process appropriately, two preliminary studies were performed separately: the kinetics of CaO–CO_2 reaction (TG technique) and investigation of the hydrodynamic characteristics of the solid-phase flow in the column at room conditions. RPM described well the carbonization kinetics both in the kinetic and product layer diffusion controlled regime. The hydrodynamic experiments showed that the more uniform radial distribution of the solid-phase can be achieved with inserting the spacings–redistributors in the column. The mean particle velocity was found independent of the gas and solid flow rates, and pressure gradient along the column was negligible. Vibrations generally improved the flowability of the solid-phase and lowered the static holdup. With the parameters obtained from the hydrodynamic and kinetic study, plug flow model for both solid- and gas-phase was proposed for the description of the countercurrent gas–solid reactive flow. The model satisfactorily described the experimental results, with the gas–solid mass-transfer coefficient predicted from the Ranz–Marshall correlation for a single particle in an undisturbed gas flow.

Acknowledgments

The authors would like to thank Slovenian Research Agency (ARRS) (Program P2–0152) for financing this work, and Sulzer Chemtech Ltd, Switzerland, for their cooperation and provision of the SMV static mixers. Their gratitude also goes to Matjaž Debeljak, the director of Solkanska Industrija Apna, Nova Gorica, Slovenia, for the donation of CaO material for this research. The authors are also grateful to Urška Kavčič for her help during the hydrodynamic experimental work, as well as dr. Gorazd Berčič for his valuable technical suggestions.

Literature Cited

1. Verver AB, van Swaaij WPM. The gas–solid trickle-flow reactor for the catalytic oxidation of hydrogen sulphide: a trickle-phase model. *Chem Eng Sci*. 1987;42:435–445.
2. Kuczynski M. *The Synthesis of Methanol in a Gas–Solid–Solid Trickle-Flow Reactor*, Ph.D. Thesis. Enschede, Netherlands: University of Twente, 1987.
3. Verver AB, van Swaaij WPM. The hydrodynamic behaviour of gas–solid trickle flow over a regularly stacked packing. *Powder Technol*. 1986;45:119–132.
4. Obradović A, Likozar B, Levec J. Catalytic surface development of novel nickel plate catalyst with combined thermally annealed platinum and alumina coatings for steam methane reforming, *Int J Hydrogen Energy*. 2013;38:1419–1429.
5. Obradović A, Likozar B, Levec J. Steam methane reforming over Ni-based pellet-type and Pt/Ni/Al_2O_3 plate-type catalyst: intrinsic kinetics study. *Ind Eng Chem Res*. 2013;52:13597–13606.
6. Thakur RK, Vial C, Nigam KDP, Nauman EB, Djelveh G. Static mixers in the process industries—a review. *Trans IchemE*. 2003;81:787–826.
7. Symonds RT, Lua DY, Macchi A, Hughes RW, Anthony EJ. CO_2 capture from syngas via cyclic carbonation/calcination for a naturally occurring limestone: modelling and bench-scale testing. *Chem Eng Sci*. 2009;64:3536–3543.
8. Harrison DP. Sorption-enhanced hydrogen production: a review. *Ind Eng Chem Res*. 2008;47:6486–6501.
9. Lee DK. An apparent kinetic model for the carbonation of calcium oxide by carbon dioxide. *Chem Eng J*. 2004;100:71–77.
10. Johnsen K, Grace JR, Elnashaie SSEH, Kolbeinsen L, Eriksen D. Modeling of sorption-enhanced steam reforming in a dual fluidized bubbling bed reactor. *Ind Eng Chem Res*. 2006;45:4133–4144.
11. Bhatia SK, Perlmutter DD. A random pore model for fluid–solid reactions: I. Isothermal, kinetic control. *AIChE J*. 1980;26:379–386.
12. Bhatia SK, Perlmutter DD. A random pore model for fluid–solid reactions: II. Diffusion and transport effects. *AIChE J*. 1981;27:247–254.
13. Heesink ABM, Prins W, van Swaaij WPM. A grain size distribution model for non-catalytic gas–solid reactions. *Chem Eng J*. 1993;53:25–37.
14. Bhatia SK, Perlmutter DD. Effect of the product layer on the kinetics of the CO_2–lime reaction. *AIChE J*. 1983;29:79–86.
15. Shimizu T, Hirama T, Hosoda H, Kitano K, Inagaki M, Tejima K. A twin fluid-bed reactor for removal of CO_2 from combustion processes. *Chem Eng Res Des*. 1999;77:62–68.
16. Grasa GS, Abanades JC, Alonso M, González B. Reactivity of highly cycled particles of CaO in a carbonation/calcination loop. *Chem Eng J*. 2008;137:561–567.
17. Dennis JS, Hayhurst AN. The effect of CO_2 on the kinetics and extent of calcination of limestone and dolomite particles in fluidised beds. *Chem Eng Sci*. 1987;42:2361–2372.
18. Grasa GS, Murillo R, Alonso M, Abanades JC. Application of the random pore model to the carbonation cyclic reaction. *AIChE J*. 2009;55(5):1246–1255.
19. Zhiming Z, Xu P, Xie M, Cheng Z, Yuan W. Modeling of the carbonation kinetics of a synthetic CaO-based sorbent. *Chem Eng Sci*. 2013;95:283–290.

20. Wakao N, Smith JM. Diffusion in catalyst pellets. *Chem Eng Sci*. 1962;17:825–834.
21. Reid RC, Prausnitz JM, Poling BE. *The Properties of Gases and Liquids*, 4th ed. McGraw-Hill, Inc., New York, 1987.
22. Bhatia SK. *The Effect of Pore Structure on the Kinetics of Fluid–Solid Reactions*, Ph.D. Thesis, University of Pennsylvania, Philadelphia, 1981.
23. Finlayson B. *The Method of Weighted Residuals and Variational Principles*. London: Academic Press, 1972.
24. Westerterp KR, Kuczynski M. Gas–solid trickle flow hydrodynamics in a packed column. *Chem Eng Sci*. 1987;42:1539–1551.
25. Roes AWM, van Swaaij WPM. Hydrodynamic behaviour of a gas–solid counter-current packed column at trickle flow. *Chem Eng J*. 1979;17:81–89.
26. Bird RB, Stewart WE, Lightfoot, EN. *Transport Phenomena. Wiley International Edition*, Wiley, New York, 1960.
27. Grasa GS, Abanades JC. CO_2 capture capacity of CaO in long series of carbonation/calcination cycles. *Ind Eng Chem Res*. 2006;45:8846–8851.
28. Alvarez D, Abanades JC. Determination of the critical product layer thickness in the reaction of CaO with CO_2. *Ind Eng Chem Res*. 2005;44:5608–5615.
29. Nikačević NM, Duduković AP. Solids residence time distribution in gas-flowing solids-fixed bed contactors. *Ind Eng Chem Res*. 2005;44:6509–6517.
30. Ranz WE, Marshall WR. Evaporation from drops. *Chem Eng Prog*. 1952;48:141–146;173–180.
31. Kiel JHA, Prins W, van Swaaij WPM. Modelling of non-catalytic reactions in a gas–solid trickle flow reactor: dry, regenerative flue gas desulphurisation using a silica-supported copper oxide sorbent. *Chem Eng Sci*. 1992;47:4271–4286.

Manuscript received July 18, 2014, and revision received Nov. 8, 2014.